

Strong spin-exchange recombination of three weakly interacting ${}^7\text{Li}$ atoms

J.-L. Li,* T. Secker, P. M. A. Mestrom, and S. J. J. M. F. Kokkelmans
 Eindhoven University of Technology, P. O. Box 513, 5600 MB Eindhoven, The Netherlands
 (Dated: July 26, 2021)

We reveal a significant spin-exchange pathway in the three-body recombination process for ultracold lithium-7 atoms near a zero-crossing of the two-body scattering length. This newly discovered recombination pathway involves the exchange of spin between all three atoms, which is not included in many theoretical approaches with restricted spin structure. Taking it into account, our calculation is in excellent agreement with experimental observations. To contrast our findings, we predict the recombination rate around a different zero-crossing without strong spin-exchange effects to be two orders of magnitude smaller, which gives a clear advantage to future many-body experiments in this regime. This work opens new avenues to study elementary reaction processes governed by the spin degree of freedom in ultracold gases.

Introduction—Weakly interacting ultracold Bose gases are an excellent testbed for fundamental many-body theories due to their theoretical simplicity and experimental controllability and tunability at a high precision level [1–3]. In most of the experimental realizations [3–9], three-body recombination (TBR) is very crucial as it constitutes a major loss source and usually determines the lifetime of the ultracold cloud. In addition, TBR has also been demonstrated to cause anti-evaporative heating [4, 5], interplay with collapse dynamics [6, 7] and is predicted to cool and even purify ultracold ensembles under particular conditions [8, 9]. So far, there have been only a few experimental investigations on TBR rates in the weak interaction regime, particularly concerning the magnetic field dependence of the TBR [10, 11]. Theoretically, quantifying TBR rates in this context is challenging and a numerical approach for it remains highly desirable.

TBR occurring in ultracold atomic gases is also a good candidate for understanding fundamental chemistry given that the reactants can be prepared in a full quantum regime with extremely high control over all external and internal degrees of freedom [12–14]. The entire reaction process has been well understood for strongly repulsive ultracold atoms for which the recombination into the shallowest molecular product is prominent [10, 15–19]. In the weak interaction regime, however, the reaction pathways for TBR can be much more complicated and the investigation of product distributions is very challenging. Early studies on this subject were established using the Jastrow approximation [20] or limited to simple systems for which only a few molecular products are involved [21, 22].

Inspiringly, experimental milestones have been achieved in the past few years by combining hy-

brid atom-ion traps and resonance-enhanced multiphoton ionization techniques [23–25]. In such experiments, chemical reaction pathways are identified on the level of full quantum state-to-state resolution regarding the electronic, vibrational, rotational, hyperfine and even magnetic quantum numbers. Several propensities in TBR processes, such as two atoms conserving their total parity, total spin and magnetic projection of total spin when forming weakly bound molecular products, are established for ${}^{87}\text{Rb}$ atoms and also explained using the hypothesis that the third atom does not flip its internal spin. Although frequently implemented in previous works for enabling three-body calculations [26–29], this hypothesis may not be generally valid, as is indicated in Ref. [30] for strongly interacting ${}^{39}\text{K}$ atoms. Therefore, whether the hypothesis and the propensities established in the ${}^{87}\text{Rb}$ system are applicable for other species remains an open question.

In this Letter, we investigate the TBR process for weakly interacting ultracold ${}^7\text{Li}$ atoms in an external magnetic field using a multichannel framework. We successfully quantify the TBR rate and identify the dominant recombination pathways. One of these pathways involves spin-exchange between the created molecule and the remaining free atom. This demonstrates the violation of the aforementioned hypothesis for ${}^7\text{Li}$ and we further analyze the origin of this violation. For comparison, we also decrease the magnetic field to study the TBR process of ${}^7\text{Li}$ atoms in the regime where spin-exchange decay processes are much less significant.

Spin models—We follow Ref. [30] to write down the Hamiltonian H_0 , describing three alkali-metal atoms at infinite separation in an external magnetic field B , as

$$H_0 = \sum_{\sigma_1 \sigma_2 \sigma_3} (T + E_{\sigma_1} + E_{\sigma_2} + E_{\sigma_3}) |\sigma_1 \sigma_2 \sigma_3\rangle \langle \sigma_1 \sigma_2 \sigma_3|, \quad (1)$$

where T is the kinetic energy operator, and E_{σ_a}

* Corresponding author: j.li1@tue.nl

and $|\sigma_a\rangle$ denote the channel energy and the corresponding internal spin state, respectively, of atom a ($a = 1, 2, 3$), which are B -dependent. Adiabatically, each state $|\sigma\rangle$ can be unambiguously traced back to a hyperfine state $|f, m_f\rangle$ at zero field, or forward to a $|m_s, m_i\rangle$ state at infinite field [31]. Here, f denotes the quantum number of atomic total spin \mathbf{f} summing up the electronic spin \mathbf{s} and nuclear spin \mathbf{i} , and m_f, m_i and m_s are the corresponding magnetic quantum numbers. Even though commonly (f, m_f) is used for labeling σ , we note that $(m_s, m_i) = \sigma$ is more appropriate in this work given that the considered magnetic fields are high.

In addition to H_0 , we assume that the three atoms interact pairwise, $V = V_{12} + V_{23} + V_{13}$. The pairwise potential

$$V_{ab} = V_{ab}^S(r_{ab})\mathcal{P}_{ab}^S + V_{ab}^T(r_{ab})\mathcal{P}_{ab}^T, \quad (2)$$

consists of singlet V_{ab}^S and triplet V_{ab}^T components in the electronic ground configuration of two alkali-metal atoms, where r_{ab} represents the distance between atom a and b and \mathcal{P}_{ab}^S (\mathcal{P}_{ab}^T) describes the projector on the electronic singlet (triplet) state of pair (a, b) . We use realistic molecular potentials for V_{ab}^S and V_{ab}^T in this work. We refer to the interaction model in Eq. (2) as the full multichannel spin (FMS) model. Several approximations can be made for simplifying the three-body calculation by restricting the way the atoms interact with each other. One frequently used restriction requires the third (spectating) atom to be fixed to the initial spin state for the other two atoms to interact, referred to as the fixed spectating spin (FSS) model in Ref. [30]. The pairwise interaction under such restriction is expressed as

$$V_{ab}^{\text{FSS}} = V_{ab}|\sigma_c^{\text{in}}\rangle\langle\sigma_c^{\text{in}}|, \quad (3)$$

where $|\sigma_c^{\text{in}}\rangle$ denotes the initial spin state of atom c and $(a, b, c) = (1, 2, 3), (2, 3, 1)$ or $(3, 1, 2)$. We also construct an optimized spin (OPS) model via

$$V_{ab}^{\text{OPS}} = \sum_{\sigma_c \in \mathcal{D}_c} V_{ab}|\sigma_c\rangle\langle\sigma_c|, \quad (4)$$

where \mathcal{D}_c represents the spin states of atom c that play a dominant role in the collision. It is apparent that the OPS model is equivalent to the FSS model when $\mathcal{D}_c \rightarrow \{\sigma_c^{\text{in}}\}$ and to the FMS model when \mathcal{D}_c includes all single-particle spin states.

Once the spin model is given, we use the Alt-Grassberger-Sandhas (AGS) equation [32] to calculate the partial TBR rate K_3^d for the decay process into a specific atom-molecule channel at zero collisional energy, see supplemental material [33]. Here, d labels both the molecule and the corresponding decay channel. The total rate, $K_3 = \sum_d K_3^d$, therefore

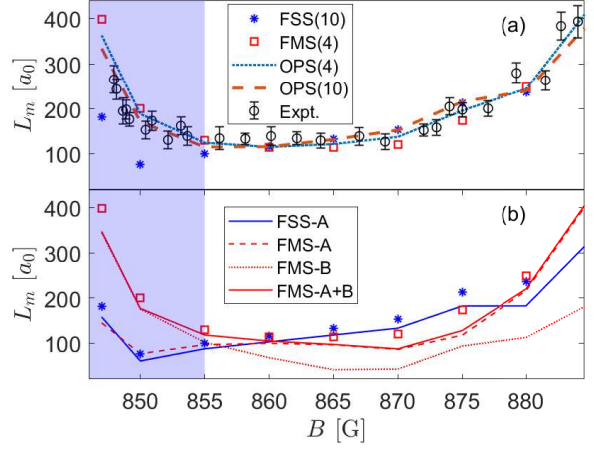


FIG. 1. (a) Three-body recombination length in units of the bohr radius a_0 for ${}^7\text{Li}$ in the $|m_s = -1/2, m_i = 1/2\rangle$ state. The stars denote the result from the FSS model with $l_{\max} = 10$ while the squares denote the results of the FMS model with $l_{\max} = 4$. The dotted and dashed lines correspond to the calculations using the OPS model with $l_{\max} = 4$ and 10, respectively. The experimental data at 2.5 μK are taken from Ref. [11]. (b) The corresponding partial contributions of the decay channels A and B in the FSS($l_{\max} = 10$) and FMS($l_{\max} = 4$) calculations. The stars and squares represent the same results as in (a). The light purple area indicates the strong three-body spin-exchange regime.

sums up all partial contributions. We define K_3 such that $dn/dt = -\frac{1}{2}K_3n^3$, where n denotes the density of the atomic gas. This definition is consistent with the one in Refs. [30, 34–36], while it differs from the one in Ref. [11] by a factor of two. In our calculations, we truncate the molecular orbital angular momentum quantum number l up to l_{\max} and implement a cut-off on the relative momentum between the atom and the molecule [33].

Strong spin-exchange TBR—We investigate a system of three ${}^7\text{Li}$ atoms at zero energy initially prepared in the same $|m_s = -1/2, m_i = 1/2\rangle$ state, which corresponds to $|f = 1, m_f = 0\rangle$ in conventional notation. We study the system in an external magnetic field varied between 847 and 885 G, covering a zero-crossing of the two-body s -wave scattering length at $B = 850$ G, where experimental data for the TBR rate are reported in Ref. [11]. The singlet and triplet potentials are taken from Ref. [37]. For comparison, we follow Ref. [11] to define the recombination length L_m via

$$K_3 = 328.2 \frac{\hbar}{m} L_m^4, \quad (5)$$

where m denotes the mass of the atom.

Figure 1(a) compares our results to the experi-

mental measurement in Ref. [11]. The result of the FMS calculation with $l_{\max} = 4$ is in excellent agreement with the experimental results at the considered magnetic fields. However, that of the FSS calculation with $l_{\max} = 10$ only agrees with experiment for $B \gtrsim 860$ G, but deviates from the experimental measurement for $B \lesssim 860$ G. The difference in performance between the two approaches does not result from the truncation of the quantum number l , since our additional FSS calculation with $l_{\max} = 4$ leads to only a small shift compared to that with $l_{\max} = 10$, not shown in Fig. 1(a) though. Therefore, we attribute the invalidity of the FSS model to its incapability to represent some important three-body channels.

By analyzing our FMS result, we find two dominant product channels, which together contribute more than 50% to the total TBR rate among more than 300 involved products in our model. We identify that one dominant product channel (decay channel A) consists of the energetically shallowest s -wave molecule with a projection quantum number of total two-body spin $M_{2b} = m_{s_a} + m_{i_a} + m_{s_b} + m_{i_b} = 0$ plus a free atom in its initial $|m_{s_c} = -1/2, m_{i_c} = 1/2\rangle$ spin state. This decay channel is included in the FSS model and the corresponding contributions to the recombination length are similar in both the FSS and FMS calculations as is shown in Fig. 1(b). However, the other dominant product channel (decay channel B) consisting of the shallowest s -wave molecule with $M_{2b} = -1$ plus a free atom in the $|m_{s_c} = -1/2, m_{i_c} = 3/2\rangle$ state is not represented in the FSS model. The spin-exchange recombination to decay channel B becomes increasingly important with decreasing magnetic field at $B \lesssim 860$ G and ultimately dominates over the one to decay channel A when $B \lesssim 855$ G, leading to a rapid enhancement of the loss rate. Moreover, its contribution matches very well with the deviation between the FSS calculation and the measurement at $B \lesssim 860$ G.

Allowing the third atom to switch from its initial $|m_{s_c} = -1/2, m_{i_c} = 1/2\rangle$ to the $|m_{s_c} = -1/2, m_{i_c} = 3/2\rangle$ spin state, we arrive at an OPS model with $\mathcal{D}_c = \{(-1/2, 1/2), (-1/2, 3/2)\}$. This OPS model gives results consistent with the measurement, when we truncate the molecular orbital angular momentum quantum number l at $l_{\max} = 4$ and 10. The results are also in line with the values we calculated with the FMS model, demonstrating again that the truncation of l has a minor influence on our calculation.

In Ref. [11], the enhancement of the TBR rate at $B \lesssim 855$ G is suggested to be governed by a two-body length scale L'_e that is determined by the two-body scattering length and effective range parameter. In contrast, our analysis demonstrates that

it originates from a single specific atom-molecule product channel coupled to the three-body incoming state via the spin-exchange recombination mechanism. In general, the two-body quantity L'_e is not able to describe this three-body spin-exchange process. It remains an open question why L'_e works beyond its capacity to explain the TBR rate qualitatively [11].

The three-body channels with $|m_{s_c} = -1/2, m_{i_c} = 3/2\rangle$ become important in the present calculation because their small energy separations to the incoming threshold lead to large multichannel couplings [30, 33]. However, the observed effect that three ${}^7\text{Li}$ atoms recombine predominantly into decay channel B seems counterintuitive at first glance since decay channel A is less separated from the three-body incoming threshold than decay channel B in the considered magnetic field regime [33]. To explain the strong recombination into decay channel B, we use an approach similar to the one in Ref. [24], in which the TBR rate to a specific decay channel is explained by the overlap of the product molecule state and a zero energy scattering state of two atoms forming that molecule. However, the original treatment of Ref. [24] is based on the hypothesis that the third atom does not flip its internal spin during the TBR process and cannot describe the recombination process into decay channel B. Therefore we extend this treatment by taking into account the interaction with the third atom and the exact three-body spin structure and study the overlap $\mathcal{O}_d = {}_\alpha \langle \psi_d | (P_+ + P_-) V_\alpha | \psi_{\text{scat}} \rangle_\alpha$ [33]. We use $\alpha = (a, b)$ to label the pair (a, b) that forms the molecule d . $|\psi_d\rangle_\alpha$ and $|\psi_{\text{scat}}\rangle_\alpha$ denote the state of molecule d plus a free atom and that of a zero-energy scattering complex of the pair (a, b) plus a free atom, respectively [38]. The interaction term $(P_+ + P_-) V_\alpha$ that couples $|\psi_{\text{scat}}\rangle_\alpha$ and $|\psi_d\rangle_\alpha$ is derived from a perturbative analysis on the AGS equation [33]. P_+ and P_- denote the cyclic and anticyclic permutation operators, respectively. We use \mathcal{O}_d to explain the dominancies of decay channels A and B as it captures the overall trend and relative magnitude of the TBR rates at the considered magnetic fields [33].

The overlaps \mathcal{O}_A and \mathcal{O}_B are written as

$$\mathcal{O}_d = 2 \sum_{\sigma_{2b}^d, \sigma_{2b}^{\text{scat}}} \mathcal{C}_{\sigma_{2b}^d \sigma_{2b}^{\text{scat}}} \langle \sigma_{2b}^d \sigma_c^d | P_+^s | \sigma_{2b}^{\text{scat}} \sigma_c^{\text{in}} \rangle, d = A, B, \quad (6)$$

where $\mathcal{C}_{\sigma_{2b}^d \sigma_{2b}^{\text{scat}}} \equiv {}_\alpha \langle \psi_d | P_+^c | \sigma_{2b}^d \sigma_c^d \rangle \langle \sigma_{2b}^{\text{scat}} \sigma_c^{\text{in}} | V_\alpha | \psi_{\text{scat}} \rangle_\alpha$ represents the spatial part of \mathcal{O}_d , which can be simplified as $\mathcal{C}_{\sigma_{2b}^d \sigma_{2b}^{\text{scat}}} = \langle \phi_d | \frac{1}{2} q_d, \sigma_{2b}^d \rangle \langle q_d, \sigma_{2b}^{\text{scat}} | V_\alpha | \phi_{\text{scat}} \rangle_\alpha$ [33]. We use P_+^s and P_+^c to denote the permutation operator P_+ acting only on the spin and coordinate space,

TABLE I. Nonzero elements of $\langle \sigma_{2b}^d \sigma_c^d | P_+^s | \sigma_{2b}^{\text{scat}} \sigma_c^{\text{in}} \rangle$ and the corresponding spin states for decay channels A and B. We use $\sigma_{2b}^A = \{\mathcal{A}_1, \mathcal{A}_2, \dots, \mathcal{A}_8\}$, $\sigma_{2b}^B = \{\mathcal{B}_1, \mathcal{B}_2, \dots, \mathcal{B}_6\}$ and $\sigma_{2b}^{\text{scat}} = \{\mathcal{S}_1, \mathcal{S}_2, \dots, \mathcal{S}_8\}$ to label these two-body spin states in the order of increasing two-body channel energy. Note that $\sigma_c^{\text{in}} = (-1/2, 1/2)$ in all cases.

d	σ_c^d	σ_{2b}^d	$\sigma_{2b}^{\text{scat}}$	$\langle \sigma_{2b}^d \sigma_c^d P_+^s \sigma_{2b}^{\text{scat}} \sigma_c^{\text{in}} \rangle$
A	$(-1/2, 1/2)$	$\mathcal{A}_1 = (-1/2, 1/2; -1/2, 1/2)$	$\mathcal{S}_1 = (-1/2, 1/2; -1/2, 1/2)$	1
A	$(-1/2, 1/2)$	$\mathcal{A}_4 = (-1/2, 1/2; 1/2, -1/2)$	$\mathcal{S}_4 = (-1/2, 1/2; 1/2, -1/2)$	1/2
B	$(-1/2, 3/2)$	$\mathcal{B}_1 = (-1/2, -1/2; -1/2, 1/2)$	$\mathcal{S}_2 = (-1/2, -1/2; -1/2, 3/2)$	1/2
B	$(-1/2, 3/2)$	$\mathcal{B}_3 = (1/2, -3/2; -1/2, 1/2)$	$\mathcal{S}_3 = (1/2, -3/2; -1/2, 3/2)$	1/2

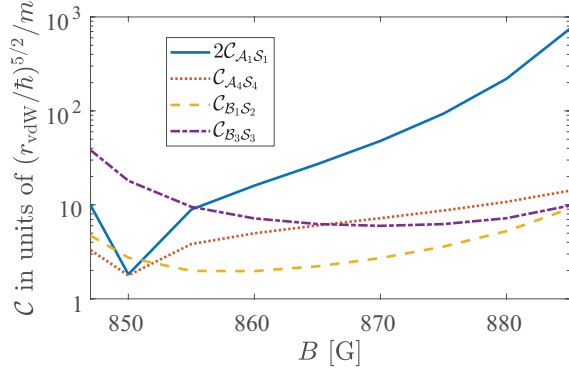


FIG. 2. Components of \mathcal{O}_A and \mathcal{O}_B as a function of magnetic field. Here r_{vdW} denotes the characteristic length scale for the van der Waals interaction between two atom [31].

and $\sigma_{2b} = (m_{s_a}, m_{i_a}; m_{s_b}, m_{i_b})$ for the spin state of the pair (a, b) . We assume that $|\sigma_{2b}\rangle$ is properly symmetrized as in Ref. [30]. Here ϕ_d and ϕ_{scat} represent the radial wave functions of molecule d and the two-body scattering state, respectively [33]. Furthermore, q_d denotes the magnitude of the relative momentum between the free atom and molecule d .

We find that the field-independent spin coupling matrix $\langle \sigma_{2b}^d \sigma_c^d | P_+^s | \sigma_{2b}^{\text{scat}} \sigma_c^{\text{in}} \rangle$ picks out only a few specific elements of \mathcal{C} that contribute to the overlap \mathcal{O}_d . For both decay channels A and B, there are only two contributions of which the corresponding spin states and spin coupling matrix elements are listed in Table I. Implementing the results of Table I into Eq. (6), we get

$$\begin{aligned} \mathcal{O}_A &= 2\mathcal{C}_{\mathcal{A}_1 \mathcal{S}_1} + \mathcal{C}_{\mathcal{A}_4 \mathcal{S}_4}, \\ \mathcal{O}_B &= \mathcal{C}_{\mathcal{B}_1 \mathcal{S}_2} + \mathcal{C}_{\mathcal{B}_3 \mathcal{S}_3}. \end{aligned} \quad (7)$$

The above expression shows explicitly that the interplay between two specific elements of the spatial part matrix \mathcal{C} determines the overlap \mathcal{O}_d . Figure 2 shows that $2\mathcal{C}_{\mathcal{A}_1 \mathcal{S}_1}$ and $\mathcal{C}_{\mathcal{B}_3 \mathcal{S}_3}$ are the most significant contributions at $B \gtrsim 855$ G and $B \lesssim 855$ G, respectively. The enhanced behavior of $2\mathcal{C}_{\mathcal{A}_1 \mathcal{S}_1}$ and

TABLE II. K_3 from the FMS and FSS models for ${}^7\text{Li}$ at $B = 850$ G (H) and $B = 578$ G (L), and for ${}^{87}\text{Rb}$ in the $|f = 1, m_f = -1\rangle$ state at $B = 1$ G. In these calculations, we take $l_{\text{max}} = 4$ for ${}^7\text{Li}$ and $l_{\text{max}} = 10$ for ${}^{87}\text{Rb}$. The numbers are presented in units of cm^6/s . The singlet and triplet potentials for ${}^{87}\text{Rb}$ are taken from Ref. [39].

Atom	FSS	FMS	Expt.
${}^7\text{Li(H)}$	1.0×10^{-27}	3.8×10^{-26}	$1.3(0.4) \times 10^{-26}$ [11]
${}^7\text{Li(L)}$	1.7×10^{-28}	1.2×10^{-28}	$< 2.3 \times 10^{-27}$ [11]
${}^{87}\text{Rb}$	4.0×10^{-29}	4.0×10^{-29}	$8.6(3.6) \times 10^{-29}$ [40]

$\mathcal{C}_{\mathcal{B}_3 \mathcal{S}_3}$ thus explains the dominance of decay channels A and B in each magnetic field regime. We find that these enhancements originate from the influence of the Feshbach resonance at $B = 894$ G on the molecular wave function ϕ_A and that of the Feshbach resonance at $B = 845$ G on the two-body scattering wave function ϕ_{scat} , respectively [33].

Lower field zero-crossing and comparison to ${}^{87}\text{Rb}$ —For comparison, we investigate the TBR rate near a different zero-crossing of the two-body scattering length at $B = 578$ G in the same spin state of ${}^7\text{Li}$ [41]. Table II shows that K_3 at $B = 850$ G is higher by two orders of magnitude than that at $B = 578$ G, where the comparable values of K_3 predicted by the FSS and FMS models indicate no strong spin-exchange process. We note that decay channel B becomes less important at $B = 578$ G [33]. However, the scenario of ${}^7\text{Li}$ at $B = 578$ G is still in contrast with the ${}^{87}\text{Rb}$ system, where the FSS and FMS calculations yield nearly identical results. Therefore, we conclude that the model with the fixed spectating atom's spin state works very well for ${}^{87}\text{Rb}$ at low magnetic fields, but not for ${}^7\text{Li}$. In general, the TBR rates from our calculation agree with experimental values [11, 40] within a factor of 2 or 3. The deviation could come from our numerical truncations or from the experimental uncertainty in the number of atoms. For instance, by implementing a larger $l_{\text{max}} = 10$ with the OPS model we get $K_3 = 2.0 \times 10^{-26} \text{ cm}^6/\text{s}$ at $B = 850$ G, which agrees better with the experimentally mea-

sured value $1.3(0.4) \times 10^{-26} \text{ cm}^6/\text{s}$ [11].

Our prediction of low TBR rate suggests that ${}^7\text{Li}$ at $B \approx 578 \text{ G}$ is a good candidate for the first realization of quantum gas purification experiments via three-body loss [9] and the creation of big time crystals [42]. Other interesting phenomena like the matter wave bright soliton [43–46] and the weak collapse of a Bose-Einstein condensate [47], which have been experimentally studied, can also be investigated in this specific case, where an extremely small slope $0.01a_0/\text{G}$ of the two-body scattering length to magnetic field leads to easy and precise control of the required weak attractive interaction.

Conclusion— We have studied the three-body recombination process of ultracold ${}^7\text{Li}$ atoms near two zero-crossings of the two-body scattering length at $B = 850 \text{ G}$ and 578 G . In the vicinity of 850 G , we get a very good agreement with the measured recombination rate and reveal a prominent spin-exchange three-body recombination pathway requir-

ing one atom to flip its nuclear spin when the other two colliding atoms form a molecule. We attribute the prominence of this pathway to the influence of the Feshbach resonance at $B = 845 \text{ G}$ on the two-body scattering wave function. The strong spin-exchange effect increases the recombination rate by about two orders of magnitude compared to our results around 578 G in the same spin state. Our approach can also be applied to other species to explore the complicated but important multichannel three-body recombination process and to analyze the rich interplay between the translational, vibrational, rotational, electronic spin and nuclear spin degrees of freedom.

Acknowledgements— We thank Lev Khaykovich, Denise Ahmed-Braun, Victor Colussi, Gijs Groeneveld, and Silvia Musolino for discussions. This research is financially supported by the Netherlands Organisation for Scientific Research (NWO) under Grant No. 680-47-623.

-
- [1] J. O. Andersen, *Rev. Mod. Phys.* **76**, 599 (2004).
 - [2] C. J. Pethick and H. Smith, *Bose-Einstein Condensation in Dilute Gases*, 2nd ed. (Cambridge University Press, 2008).
 - [3] I. Bloch, J. Dalibard, and W. Zwerger, *Rev. Mod. Phys.* **80**, 885 (2008).
 - [4] T. Weber, J. Herbig, M. Mark, H.-C. Nägerl, and R. Grimm, *Phys. Rev. Lett.* **91**, 123201 (2003).
 - [5] U. Eismann, L. Khaykovich, S. Laurent, I. Ferrier-Barbut, B. S. Rem, A. T. Grier, M. Delehaye, F. Chevy, C. Salomon, L.-C. Ha, and C. Chin, *Phys. Rev. X* **6**, 021025 (2016).
 - [6] E. A. Donley, N. R. Claussen, S. L. Cornish, J. L. Roberts, E. A. Cornell, and C. E. Wieman, *Nature* **412**, 295 (2001).
 - [7] P. A. Altin, G. R. Dennis, G. D. McDonald, D. Döring, J. E. Debs, J. D. Close, C. M. Savage, and N. P. Robins, *Phys. Rev. A* **84**, 033632 (2011).
 - [8] M. Schemmer and I. Bouchoule, *Phys. Rev. Lett.* **121**, 200401 (2018).
 - [9] L. H. Dogra, J. A. P. Glidden, T. A. Hilker, C. Eigen, E. A. Cornell, R. P. Smith, and Z. Hadzibabic, *Phys. Rev. Lett.* **123**, 020405 (2019).
 - [10] T. Kraemer, M. Mark, P. Waldburger, J. Danzl, C. Chin, B. Engeser, K. Pilch, A. Jaakkola, H.-C. Nägerl, and R. Grimm, *Nature* **440**, 315 (2006).
 - [11] Z. Shotan, O. Machtey, S. Kokkelmans, and L. Khaykovich, *Phys. Rev. Lett.* **113**, 053202 (2014).
 - [12] N. Balakrishnan, *The Journal of Chemical Physics* **145**, 150901 (2016).
 - [13] G. Quéméner and P. S. Julienne, *Chemical Reviews* **112**, 4949 (2012).
 - [14] C. H. Greene, P. Giannakeas, and J. Pérez-Ríos, *Rev. Mod. Phys.* **89**, 035006 (2017).
 - [15] E. Braaten and H.-W. Hammer, *Physics Reports* **428**, 259 (2006).
 - [16] S. E. Pollack, D. Dries, and R. G. Hulet, *Science* **326**, 1683 (2009).
 - [17] N. Gross, Z. Shotan, S. Kokkelmans, and L. Khaykovich, *Phys. Rev. Lett.* **103**, 163202 (2009).
 - [18] N. Gross, Z. Shotan, S. Kokkelmans, and L. Khaykovich, *Phys. Rev. Lett.* **105**, 103203 (2010).
 - [19] M. Zaccanti, B. Deissler, C. D’Errico, M. Fattori, M. Jona-Lasinio, S. Müller, G. Roati, M. Inguscio, and G. Modugno, *Nature Physics* **5**, 586 (2009).
 - [20] A. J. Moerdijk, H. M. J. M. Boesten, and B. J. Verhaar, *Phys. Rev. A* **53**, 916 (1996).
 - [21] Y. Wang, J. P. D’Incao, and B. D. Esry, *Phys. Rev. A* **83**, 032703 (2011).
 - [22] H. Suno and B. D. Esry, *Phys. Rev. A* **80**, 062702 (2009).
 - [23] A. Härter, A. Krüchow, M. Deiß, B. Drews, E. Tiemann, and J. H. Denschlag, *Nature Physics* **9**, 512 (2013).
 - [24] J. Wolf, M. Deiß, A. Krüchow, E. Tiemann, B. P. Ruzic, Y. Wang, J. P. D’Incao, P. S. Julienne, and J. H. Denschlag, *Science* **358**, 921 (2017).
 - [25] J. Wolf, M. Deiß, and J. Hecker Denschlag, *Phys. Rev. Lett.* **123**, 253401 (2019).
 - [26] Y. Wang and P. S. Julienne, *Nature Physics* **10**, 768 (2014).
 - [27] K. Kato, Y. Wang, J. Kobayashi, P. S. Julienne, and S. Inouye, *Phys. Rev. Lett.* **118**, 163401 (2017).
 - [28] R. Chapurin, X. Xie, M. J. Van de Graaff, J. S. Popowski, J. P. D’Incao, P. S. Julienne, J. Ye, and E. A. Cornell, *Phys. Rev. Lett.* **123**, 233402 (2019).
 - [29] X. Xie, M. J. Van de Graaff, R. Chapurin, M. D. Frye, J. M. Hutson, J. P. D’Incao, P. S. Julienne, J. Ye, and E. A. Cornell, *Phys. Rev. Lett.* **125**, 243401 (2020).

- [30] T. Secker, J.-L. Li, P. M. A. Mestrom, and S. J. J. M. F. Kokkelmans, *Phys. Rev. A* **103**, 022825 (2021).
- [31] C. Chin, R. Grimm, P. Julienne, and E. Tiesinga, *Rev. Mod. Phys.* **82**, 1225 (2010).
- [32] E. Alt, P. Grassberger, and W. Sandhas, *Nuclear Physics B* **2**, 167 (1967).
- [33] See Supplemental Material for additional details of our calculations, derivations and results, which includes Refs. [48–50].
- [34] E. Braaten, H.-W. Hammer, D. Kang, and L. Platter, *Phys. Rev. A* **78**, 043605 (2008).
- [35] P. M. A. Mestrom, T. Secker, R. M. Kroeze, and S. J. J. M. F. Kokkelmans, *Phys. Rev. A* **99**, 012702 (2019).
- [36] T. Secker, J.-L. Li, P. M. A. Mestrom, and S. J. J. M. F. Kokkelmans, *Phys. Rev. A* **103**, 032817 (2021).
- [37] P. S. Julienne and J. M. Hutson, *Phys. Rev. A* **89**, 052715 (2014).
- [38] One should not confuse $|\psi_{\text{scat}}\rangle_\alpha$ with the system's real initial state $|\psi_{\text{in}}\rangle$ describing three free atoms.
- [39] C. Strauss, T. Takekoshi, F. Lang, K. Winkler, R. Grimm, J. Hecker Denschlag, and E. Tiemann, *Phys. Rev. A* **82**, 052514 (2010).
- [40] E. A. Burt, R. W. Ghrist, C. J. Myatt, M. J. Holland, E. A. Cornell, and C. E. Wieman, *Phys. Rev. Lett.* **79**, 337 (1997).
- [41] The small discrepancy between our calculated magnetic field value $B = 578$ G of this zero crossing and the value $B \approx 576$ G given by Ref. [11] comes from slight differences in the interaction potentials employed in both calculations. The effect of this discrepancy on the three-body recombination rate is negligible.
- [42] K. Giergiel, T. Tran, A. Zaheer, A. Singh, A. Sidorov, K. Sacha, and P. Hannaford, *New Journal of Physics* **22**, 085004 (2020).
- [43] L. Khaykovich, F. Schreck, G. Ferrari, T. Bourdel, J. Cubizolles, L. D. Carr, Y. Castin, and C. Salomon, *Science* **296**, 1290 (2002).
- [44] K. E. Strecker, G. B. Partridge, A. G. Truscott, and R. G. Hulet, *Nature* **417**, 150 (2002).
- [45] J. H. V. Nguyen, P. Dyke, D. Luo, B. A. Malomed, and R. G. Hulet, *Nature Physics* **10**, 918 (2014).
- [46] D. Luo, Y. Jin, J. H. V. Nguyen, B. A. Malomed, O. V. Marchukov, V. A. Yurovsky, V. Dunjko, M. Olshanii, and R. G. Hulet, *Phys. Rev. Lett.* **125**, 183902 (2020).
- [47] C. Eigen, A. L. Gaunt, A. Suleymanzade, N. Navon, Z. Hadzibabic, and R. P. Smith, *Phys. Rev. X* **6**, 041058 (2016).
- [48] M. D. Lee, T. Köhler, and P. S. Julienne, *Phys. Rev. A* **76**, 012720 (2007).
- [49] D. J. Ernst, C. M. Shakin, and R. M. Thaler, *Phys. Rev. C* **8**, 46 (1973).
- [50] L. Hlophe, C. Elster, R. C. Johnson, N. J. Upadhyay, F. M. Nunes, G. Arbanas, V. Eremenko, J. E. Escher, and I. J. Thompson (TORUS Collaboration), *Phys. Rev. C* **88**, 064608 (2013).

Supplemental Material: “Strong spin-exchange recombination of three weakly interacting ${}^7\text{Li}$ atoms”

J.-L. Li, T. Secker, P. M. A. Mestrom, and S. J. J. M. F. Kokkelmans

Eindhoven University of Technology, P. O. Box 513, 5600 MB Eindhoven, The Netherlands

(Dated: July 26, 2021)

I. AGS EQUATION AND TBR RATE

We solve the AGS equation in momentum space [30, 35, 36, 48]

$$U_{\alpha 0}(z) = \frac{1}{3}G_0^{-1}(z)[1 + P_+ + P_-] + [P_+ + P_-]\mathcal{T}_\alpha(z)G_0(z)U_{\alpha 0}(z). \quad (\text{S1})$$

via a numerical approach combining the separable expansion method and the two-body mapped grid technique [30, 36]. Here $G_0 = (z - H_0)^{-1}$ is the free Green’s operator and $\mathcal{T}_\alpha = (1 - V_\alpha G_0(z))^{-1}V_\alpha$ represents the generalized two-body transition operator for the pair $\alpha = (a, b)$. P_+ and P_- denote the cyclic and anticyclic permutation operators, respectively. The three-body transition operator $U_{\alpha 0}$, whose elements describe the transition probabilities from the initial free-atom state to product states of a molecule plus a free atom, is closely related to the TBR rate K_3 . In this paper, we define the partial recombination rate K_3^d to each specific molecular product d as [30, 35, 36, 48]

$$K_3^d = \frac{24\pi m}{\hbar}(2\pi\hbar)^6 q_d |\alpha \langle \psi_d | U_{\alpha 0}(z) | \psi_{\text{in}} \rangle|^2, \quad (\text{S2})$$

where $|\psi_{\text{in}}\rangle$ and $|\psi_d\rangle$ represent the initial and product states, respectively. q_d is the magnitude of the momentum of the free atom relative to the center of mass of molecule d . In our calculations, we take the zero energy limit $z \rightarrow 0$ from the upper half of the complex energy plane and therefore fix the total orbital angular momentum quantum number $J = 0$. The projection quantum number of the total spin angular momentum $M_{\text{tot}} = \sum_a m_{s_a} + \sum_a m_{i_a}$ ($a = 1, 2$ and 3) should also be fixed during the scattering process. We also implement truncations l_{max} on the orbital angular momentum quantum number l related to the relative movement of the atoms constituting the molecule and q_{max} on the magnitude of the momentum q of the third atom relative to the molecule’s center of mass. In particular, $q_{\text{max}} = 20 \hbar/r_{\text{vdW}}$ is used throughout the entire paper and l_{max} is stated explicitly when the results are presented in the main text. It is worth noting that the sufficiency of $q_{\text{max}} = 20 \hbar/r_{\text{vdW}}$ is demonstrated for addressing the three-body parameter in Refs. [30, 36] and additionally checked for our present study by comparing to a larger cutoff $q_{\text{max}} = 40 \hbar/r_{\text{vdW}}$. For more

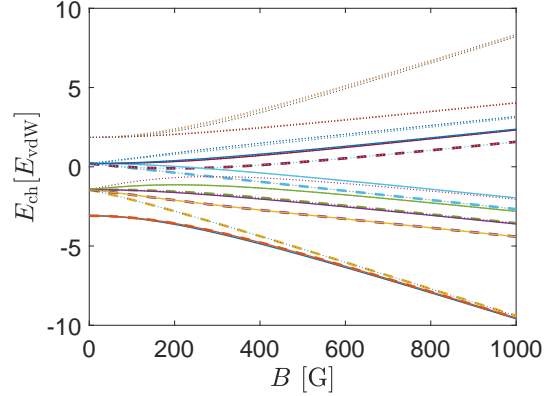


FIG. S1. Channel energy E_{ch} in units of $E_{\text{vdW}} = \hbar^2/(mr_{\text{vdW}}^2)$ of three ${}^7\text{Li}$ atoms with $M_{\text{tot}} = 0$. The solid and dashed lines represent the three-body channels with $\sigma_c = (-1/2, 1/2)$ and $(-1/2, 3/2)$, respectively. The dotted lines correspond to other σ_c . The incoming three-body channel is the lowest one.

details about our numerical approach, we refer the reader to Refs. [30, 36].

II. THREE-BODY CHANNEL ENERGY

Figure S1 shows the three-body channel energy $E_{\text{ch}} = E_a + E_b + E_c$ with $M_{\text{tot}} = 0$ for ${}^7\text{Li}$ atoms. One can see that the channel energy separations are in general smaller than those for ${}^{39}\text{K}$ atoms [30]. In particular for those with $\sigma_c = (-1/2, 3/2)$, the two lowest channels are extremely close, with energy separations less than $0.25 E_{\text{vdW}}$, to the three-body incoming channel when $B > 800$ G. According to the analysis in Ref. [30], this can lead to strong multichannel couplings to the incoming channel.

III. ASYMPTOTIC ENERGY OF DECAY CHANNELS A AND B

To illustrate the energy separations of the product channels from the incoming channel, we calculate $\Delta E_d = E_{2b}^d + E_{\sigma_c^d} - E_{\sigma_a^{\text{in}}} - E_{\sigma_b^{\text{in}}} - E_{\sigma_c^{\text{in}}}$ for $d = A$ or B , where E_{2b}^d denotes the energy level of molecule

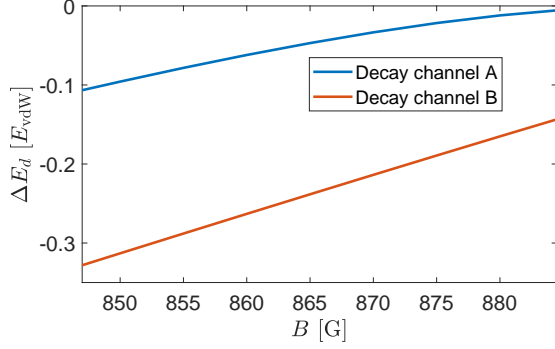


FIG. S2. Energy separations ΔE_d of decay channels A and B from the incoming threshold as a function of magnetic field.

d and $E_{\sigma_c^d}$ represents the corresponding shift due to the third atom. In the zero energy limit consid-

ered in this work, ΔE_d is simply connected to q_d via $\Delta E_d = -3q_d^2/4m$. Figure S2 shows the energy levels of both decay channels are shifted towards the incoming threshold with the increase of the magnetic field and $|\Delta E_A|$ persists to be smaller than $|\Delta E_B|$ in the considered magnetic field regime. These energy separations explain the dominance of decay channel A at $B \gtrsim 860$ G. However, it is in contrast with our observation that K_3^B is much larger than K_3^A at $B \lesssim 855$ G.

IV. TBR RATE FROM \mathcal{O}_d

To get the expression of \mathcal{O}_d in the main text, we rewrite Eq. (S1) as

$$U_{\alpha 0}(z) = \sum_{n=0}^{\infty} U_{\alpha 0}^{(n)}(z) \quad (\text{S3})$$

with

$$U_{\alpha 0}^{(n)}(z) = \{[P_+ + P_-] \mathcal{T}_\alpha(z) G_0(z)\}^n \frac{1}{3} G_0^{-1}(z) [1 + P_+ + P_-]. \quad (\text{S4})$$

Since ${}_\alpha \langle \psi_d | U_{\alpha 0}^{(0)}(z) | \psi_{\text{in}} \rangle$ vanishes at zero energy, we look into the next order term $U_{\alpha 0}^{(1)}(z)$. The initial free atom state is taken as $|\psi_{\text{in}}\rangle = |\mathbf{p} = \mathbf{0}, \mathbf{q} = \mathbf{0}\rangle |\sigma_a^{\text{in}} \sigma_b^{\text{in}} \sigma_c^{\text{in}}\rangle$, where \mathbf{p} and \mathbf{q} are Jacobi momenta corresponding to the relative motion between two atoms and that of the third atom to the center of mass of them, respectively. $|\psi_{\text{in}}\rangle$ is fully symmetric so that

$$U_{\alpha 0}^{(1)}(z) |\psi_{\text{in}}\rangle = [P_+ + P_-] \mathcal{T}_\alpha(z) |\psi_{\text{in}}\rangle. \quad (\text{S5})$$

We implement the partial wave expansion and switch from the plane wave basis $|\mathbf{p}, \mathbf{q}\rangle$ to

$|p, q\rangle |lLJM_J\rangle$, where l and L are partial wave quantum numbers corresponding to \mathbf{p} and \mathbf{q} , respectively. The initial and product states can then be expressed as $|\psi_{\text{in}}\rangle = \frac{1}{4\pi} |p=0, q=0\rangle |0000\rangle |\sigma_a^{\text{in}} \sigma_b^{\text{in}} \sigma_c^{\text{in}}\rangle$ and $|\psi_d\rangle_\alpha = |\phi_d, q_d\rangle_\alpha |l_d l_d 00\rangle |\sigma_c^d\rangle$, where ϕ_d denotes the radial wave function of molecule d . We define $|\psi_{\text{scat}}\rangle_\alpha \equiv |\phi_{\text{scat}}, q=0\rangle_\alpha |0000\rangle |\sigma_c^{\text{in}}\rangle$ to describe the state of a scattering complex plus a free atom, where ϕ_{scat} is the radial two-body scattering wave function at zero energy. Using these states and Eq. (S5), we get

$$\begin{aligned} {}_\alpha \langle \psi_d | U_{\alpha 0}^{(1)}(0) | \psi_{\text{in}} \rangle &= \frac{1}{4\pi} {}_\alpha \langle \psi_d | [P_+ + P_-] \mathcal{T}_\alpha(0) | p=0, q=0 \rangle |0000\rangle |\sigma_a^{\text{in}} \sigma_b^{\text{in}} \sigma_c^{\text{in}}\rangle \\ &= \frac{1}{4\pi} {}_\alpha \langle \psi_d | [P_+ + P_-] V_\alpha | \phi_{\text{scat}}, q=0 \rangle |0000\rangle |\sigma_c^{\text{in}}\rangle \\ &= \frac{1}{4\pi} \mathcal{O}_d \end{aligned} \quad (\text{S6})$$

with

$$\begin{aligned} \mathcal{O}_d &= {}_\alpha \langle \psi_d | [P_+ + P_-] V_\alpha | \psi_{\text{scat}} \rangle_\alpha \\ &= 2 \sum_{\sigma_{2b}^d, \sigma_{2b}^{\text{scat}}} {}_\alpha \langle \psi_d | P_+ | \sigma_{2b}^d \sigma_c^d \rangle \langle \sigma_{2b}^{\text{scat}} \sigma_c^{\text{in}} | V_\alpha | \psi_{\text{scat}} \rangle_\alpha \langle \sigma_{2b}^d \sigma_c^d | P_- | \sigma_{2b}^{\text{scat}} \sigma_c^{\text{in}} \rangle \end{aligned}$$

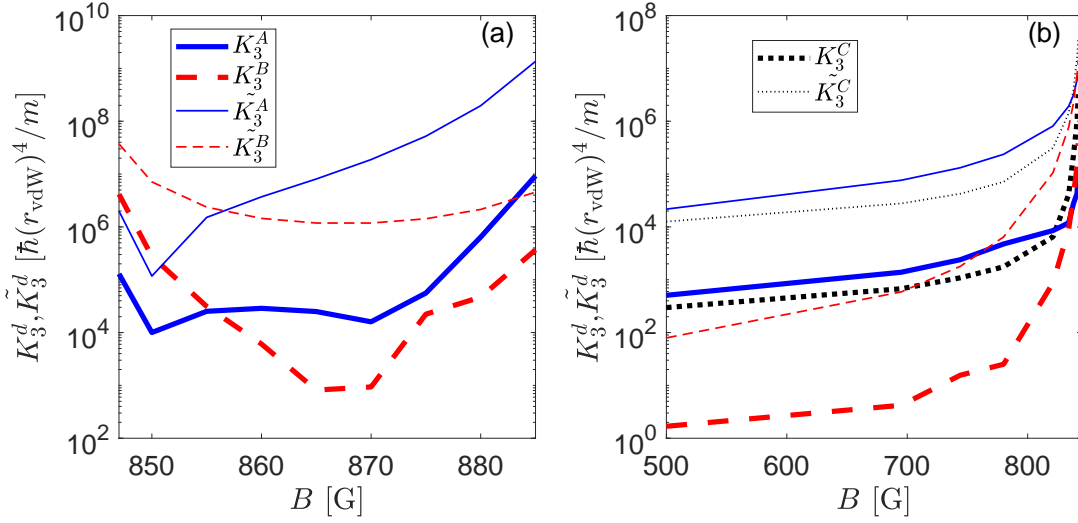


FIG. S3. The TBR rates for decay channels A, B and C calculated from $U_{\alpha 0}$ by using the FMS model with $l_{\max} = 4$ (K_3^d) and from $U_{\alpha 0}^{(1)}$ by using \mathcal{O}_d (K_3^d).

$$\begin{aligned}
&= 2 \sum_{\sigma_{2b}^d, \sigma_{2b}^{\text{scat}}} \int d\mathbf{q}' \int d\mathbf{q}''_{\alpha} \langle \psi_d | \mathbf{q}'' + \frac{1}{2}\mathbf{q}', \mathbf{q}' \rangle | \sigma_{2b}^d \sigma_c^d \rangle \langle \sigma_{2b}^{\text{scat}} \sigma_c^{\text{in}} | \langle -\mathbf{q}' - \frac{1}{2}\mathbf{q}'', \mathbf{q}'' | V_{\alpha} | \psi_{\text{scat}} \rangle_{\alpha} \langle \sigma_{2b}^d \sigma_c^d | P_{+}^{\text{s}} | \sigma_{2b}^{\text{scat}} \sigma_c^{\text{in}} \rangle \\
&= 2\sqrt{2l_d + 1} \sum_{\sigma_{2b}^d, \sigma_{2b}^{\text{scat}}} \langle \sigma_c^d |_{\alpha} \langle \phi_d | \frac{1}{2}q_d, \sigma_{2b}^d \sigma_c^d \rangle \langle q_d, \sigma_{2b}^{\text{scat}} \sigma_c^{\text{in}} | V_{\alpha} | \phi_{\text{scat}} \rangle_{\alpha} | \sigma_c^{\text{in}} \rangle \langle \sigma_{2b}^d \sigma_c^d | P_{+}^{\text{s}} | \sigma_{2b}^{\text{scat}} \sigma_c^{\text{in}} \rangle \\
&= 2\sqrt{2l_d + 1} \sum_{\sigma_{2b}^d, \sigma_{2b}^{\text{scat}}} \alpha \langle \phi_d | \frac{1}{2}q_d, \sigma_{2b}^d \rangle \langle q_d, \sigma_{2b}^{\text{scat}} | V_{\alpha} | \phi_{\text{scat}} \rangle_{\alpha} \langle \sigma_{2b}^d \sigma_c^d | P_{+}^{\text{s}} | \sigma_{2b}^{\text{scat}} \sigma_c^{\text{scat}} \rangle \\
&= 2\sqrt{2l_d + 1} \sum_{\sigma_{2b}^d, \sigma_{2b}^{\text{scat}}} \phi_d^{\sigma_{2b}^d} \left(\frac{1}{2}q_d \right) t_h^{\sigma_{2b}^{\text{scat}}} (q_d) \langle \sigma_{2b}^d \sigma_c^d | P_{+}^{\text{s}} | \sigma_{2b}^{\text{scat}} \sigma_c^{\text{in}} \rangle, \tag{S7}
\end{aligned}$$

where

$$t_h^{\sigma_{2b}^{\text{scat}}} (q_d) = \langle q_d, \sigma_{2b}^{\text{scat}} | V_{\alpha} | \phi_{\text{scat}} \rangle_{\alpha} = \langle \sigma_{2b}^{\text{scat}} | \langle p = q_d | t_{\alpha}^{l=0} (z_{2b} = 0) | p_z = 0 \rangle | \sigma_a^{\text{in}} \sigma_b^{\text{in}} \rangle \tag{S8}$$

is an element of the two-body s -wave t -matrix $t^{l=0}$ at two-body energy $z_{2b} = p_z^2/m = 0$ with one momentum fixed on the energy shell, which is commonly referred to as the half-shell t -matrix in nuclear physics [49, 50]. The expression of Eq. (6) in the main text is obtained by filling in $l_d = 0$ for $d = A$ or B in Eq. (S7).

Figure S3(a) shows that the TBR rates calculated from \mathcal{O}_d follow the overall trend of those given by the FMS calculation with $l_{\max} = 4$ in our considered magnetic field regime. The main feature that three free atoms recombine predominantly into decay channel B at $B \lesssim 855$ G and into decay channel A at $B \gtrsim 855$ G is captured by \mathcal{O}_d . Similarly, \mathcal{O}_d captures the overall trend and relative magnitude of the TBR rates near a different zero crossing at

$B = 578$ G, as is shown in Fig. S3(b). However, the absolute magnitude of the TBR rates cannot be correctly addressed by \mathcal{O}_d , indicating that our multichannel numerical calculation is indispensable for quantifying the TBR rates. Figure S3(b) also demonstrates that the spin-exchange recombination pathway to decay channel B is strongly suppressed near the zero crossing at $B = 578$ G. We note that decay channel C in Fig. S3(b) corresponds to the new shallow molecule with $M_{2b} = 0$ appearing when the magnetic field decreases over the Feshbach resonance position at $B = 845$ G.

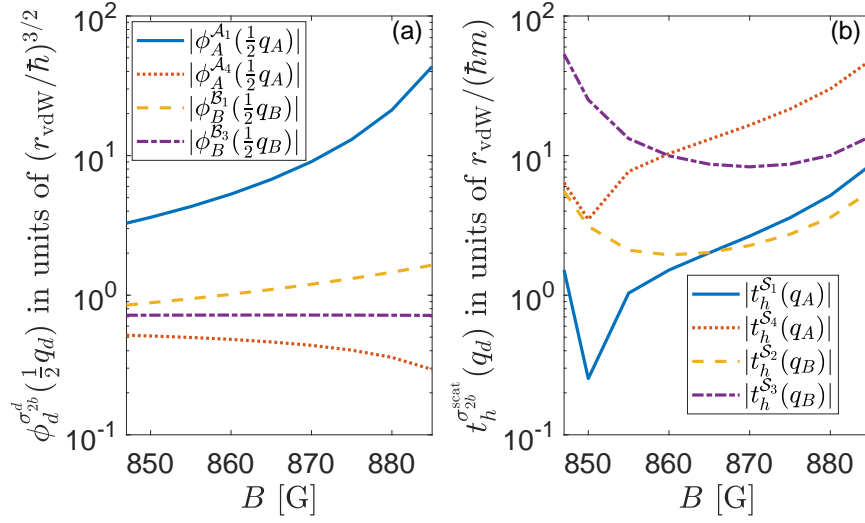


FIG. S4. The molecular wave function evaluated at $\frac{1}{2}q_d$ (a) and half-shell t -matrix evaluated at q_d (b) relevant for the overlaps \mathcal{O}_A and \mathcal{O}_B .

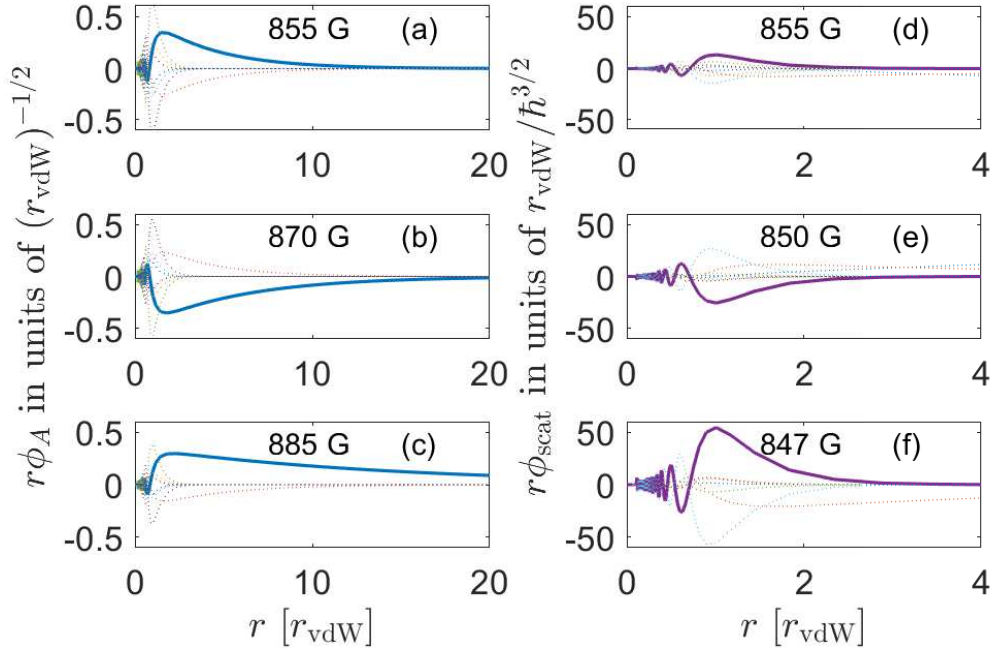


FIG. S5. (a)-(c) show the molecular wave function ϕ_A at $B = 855, 870$ and 885 G. (d)-(f) show the two-body scattering wave function ϕ_{scat} at $B = 855, 850$ and 847 G. The solid lines highlight the $\sigma_{2b}^{A_1}$ component for ϕ_A in (a)-(c) and the $\sigma_{2b}^{B_3}$ component for ϕ_{scat} in (d)-(f).

V. ANALYSIS ON $\mathcal{C}_{A_1S_1}$ AND $\mathcal{C}_{B_3S_3}$

We have demonstrated in the main text that \mathcal{O}_A is determined by $\mathcal{C}_{A_1S_1}$ at $B \gtrsim 855$ G and \mathcal{O}_B is determined by $\mathcal{C}_{B_3S_3}$ at $B \lesssim 855$ G. Now we want

to analyze which quantities make these two components the most significant. For that we write $\mathcal{C}_{A_1S_1}$

and $\mathcal{C}_{\mathcal{B}_3\mathcal{S}_3}$ as

$$\begin{aligned}\mathcal{C}_{\mathcal{A}_1\mathcal{S}_1} &= \phi_A^{\mathcal{A}_1}\left(\frac{1}{2}q_A\right)t_h^{\mathcal{S}_1}(q_A), \\ \mathcal{C}_{\mathcal{B}_3\mathcal{S}_3} &= \phi_B^{\mathcal{B}_3}\left(\frac{1}{2}q_B\right)t_h^{\mathcal{S}_3}(q_A).\end{aligned}\quad (\text{S9})$$

Figure S4(a) shows that the large value of $\mathcal{C}_{\mathcal{A}_1\mathcal{S}_1}$ at $B \gtrsim 855$ G comes from $\phi_A^{\mathcal{A}_1}(\frac{1}{2}q_A)$. The increasing behavior of $\phi_A^{\mathcal{A}_1}(\frac{1}{2}q_A)$ with the increase of magnetic field can be understood as follows. Molecule A becomes increasingly extended in the \mathcal{A}_1 channel when its energy level is shifted towards the threshold of that channel. Eventually, the energy level of molecule A merges with the threshold of the \mathcal{A}_1 channel at the Feshbach resonance position of $B = 894$ G. As a result, ϕ_A increases the amplitude of its \mathcal{A}_1 component in the large-distance (or equivalently, low-momentum) regime, as is shown in Figs. S5(a)-S5(c). In combination with a simultane-

ously decreasing q_A , this leads to a rapid increase of $\phi_A^{\mathcal{A}_1}(\frac{1}{2}q_A)$.

In contrast, the enhancement of $\mathcal{C}_{\mathcal{B}_3\mathcal{S}_3}$ at $B \lesssim 855$ G with the decreasing magnetic field comes from that of $t_h^{\mathcal{S}_3}(q_B)$, as is shown in Fig. S4(b). The behavior of $t_h^{\mathcal{S}_3}(q_B)$ at $B \lesssim 855$ G can be related to the Feshbach resonance at $B = 845$ G. In the vicinity of this Feshbach resonance, the two-body scattering state $|\phi_{\text{scat}}\rangle$ increases the amplitudes of its closed channel components at short range due to the coupling from the resonant molecular state, as is shown in Figs. S5(d)-S5(f). This leads to an enhanced component of the two-body half-shell t -matrix in the corresponding closed channels. In the present case, \mathcal{S}_3 is one of the closed channels with enhanced components. Therefore $t_h^{\mathcal{S}_3}(q_B)$ increases when the magnetic field is tuned towards the Feshbach resonance at $B = 845$ G. Similarly, $t_h^{\mathcal{S}_3}(q_B)$ is also enhanced in the vicinity of the Feshbach resonance at $B = 894$ G.